Spectroscopic, structural and DFT studies of luminescent Pt(II) and Ag(I) complexes with an asymmetric 2,2'-bipyridine chelating ligand

İsmail Yılmaz[a], Nursel S Acar[b], Simon J Coles[c], Fatih Pekdemir[d], and Abdurrahman Şengül[d,*]

[a] *Department of Chemistry, Faculty of Sciences, Karabük University, 78050 Karabük, Turkey*
[b] *Department of Chemistry, Faculty of Science, Ege University, 35100, Bornova, Izmir, Turkey*
[c] *UK National Crystallography Service, School of Chemistry, Faculty of Engineering and Physical Sciences, University of Southampton, Southampton, SO17 1BJ, UK*
[d] *Department of Chemistry, Faculty of Arts and Sciences, Zonguldak Bülent Ecevit University, 67100 Zonguldak, Turkey*

Abstract

A new unsymmetrically substituted 2,2'-bipyridine ligand, 5-methyl-5'-carbomethoxy-2,2'-bipyridine (L) was isolated from the dry distillation of the copper(II) complex, *mono*-aqua-*bis*(*trans*-5-methyl-pyridine-2-carboxylato-*N*,*O*)copper(II). The ligand was fully characterized. The spectroscopic and single-crystal X-ray diffraction (SCXRD) studies of the coordination compounds of the ligand with platinum(II) and silver(I); *cis*-Pt(L)Cl_2 (**1**) and [Ag(L)$_2$]PF_6 (**2**), respectively are reported. In **1**, the Pt centre coordinates to tertiary N atoms of the ligand and two chloride ions to form a neutral square-planar coordination sphere, while in **2**, the Ag(I) centre is coordinated by two ligands through N atoms to generate a cationic flattened tetrahedron geometry in which two mean planes intersect each other at 50.93°. The pyridine rings are nearly coplanar as revealed by the torsion angle [N1-C5-C6-N3] of 0.32°. In both complexes, L acts as a chelating ligand through pyridyl N atoms. In **1**, the molecular units are stacked in a head-to-tail fashion with a

Pt···Pt separation of 3.5 Å. Supramolecular self-assembly of the molecular units by extensive intermolecular contacts through C–H···Cl and C–H···O between the adjacent units results in an infinite two-dimensional flattened-out herringbone structure in the crystalline state. In **2**, the molecular units are interconnected with each other by C–H···O contacts between the adjacent units running parallel to each other. Both complexes are fluorescent in solution and have emission maxima in the UV-Vis regions, which is a very important property for optoelectronic applications. DFT (density functional theory) and TD-DFT (time-dependent-DFT) calculations were performed at B3LYP/6-311+G(d,p)/LANL2DZ level to explore structural, electronic, and spectroscopic properties to compare with the experimental results. The molecular orbitals (MOs) were carried out with DFT at the same level.

Keywords: Bipyridine; Platinum; Silver; Luminescence; X-ray structures, DFT studies

1. Introduction

Luminescent compounds are of current interest due to their promising applications in chemical sensors, photochemistry, and electroluminescent devices [1–7]. Metal complexes of *N*-heterocycles derived from 2,2'-bipyridine (bpy), 1,10-phenanthroline (phen) and 2,2':6',2''-terpyridine (terpy) are widely used luminophores. The optical properties of these compounds can be easily tuned by changing the nature of its substituents, protonation, and also metal complexation [8]. It has previously been shown that the presence of substituents at 5,5'-positions of 2,2'-bipyridine causes a significant red-shift of the emission maximum akin to that of the protonated ligand [8]. The main

interactions in these molecules occur by an intramolecular charge-transfer (ICT) between the donor (D) and acceptor (A) functionalities, thereby tuning the optical properties [9]. The bpy derivatives are very promising candidates as a fluorescent probe, a property that is associated with the orbital energy of the lowest unoccupied molecular orbital (LUMO) of pyridine [9]. As both a σ-donor and π-acceptor ligand, 2,2′-bipyridine derivatives form very stable metal complexes due to the formation of a five-membered ring [10]. Depending on the metal centre, 2,2′-bipyridines adopt diverse coordination geometries such as square-planar (SP), tetrahedral, and octahedral coordination geometries[10]. The syntheses of luminophores based on the 5,5′-disubstituted-2,2′-bipyridine derivatives have been reviewed previously [11]. The ligand incorporating different substituents at 5,5′-positions and their complexes with different metal ions (Pt^{II} as d^8 and Ag^{I} as d^{10} ion) will generate subtly different electronic structure and symmetry could therefore potentially give rise to tunable optical and photonic properties as reported for the analogous compounds [12]. The significant efforts on both computational and experimental studies on the asymmetric 2,2′-bipyridine derivatives [12] have stimulated us to employ DFT and TD-DFT calculations to estimate the frontier molecular orbitals (FMOs) and natural bond orbital (NBO) of these compounds. It is noteworthy that the coordination chemistry of silver(I) is very rich, showing the adoption of a wide variety of coordination geometries [13]. This rich coordination behaviour of silver(I) can be accounted for by the lack of stereochemical preference of a d^{10} configuration and the weak nature of the silver-ligand bond [14]. Ag(I) complexes with bpy type ligands emit weak photoluminescence at low temperatures due to intra-ligand emission [14]. Since the most intense electronic transition of the bpy skeleton is polarized along with the 5,5′-positions [15], the platinum(II) complexes formed with these luminophores would be very

interesting. The platinum(II) complexes with α-diimine ligands are well-known to show triplet metal-to-ligand charge-transfer (^{3}MLCT) lowest excited states [16]. Moreover, the electron-withdrawing carbomethoxy substituents on the bpy have been reported to lead to a redshift of the MLCT band [16]. Studies showed that to promote luminescence in platinum(II) complexes, the lowest-lying excited state is supposed to be a ligand-centred or charge-transfer state [17]. The electronic and spectroscopic properties of four-coordinate planar platinum(II) complexes very much depend on intermolecular, metal-metal, and also π-π interactions [18]. Herein we therefore explore the ligating properties of 5-methyl-5'-carbomethoxy-2,2'-bipyridine (L) with platinum(II) and silver(I) for the first time (Scheme 1). The corresponding metal complexes, **1** and **2** have been synthesized in the crystal form and characterized by UV-Vis, luminescence, FT-IR, ^{1}H NMR, mass and elemental analysis methods. The SCXRD analysis reveals that, despite the same chelating mode adopted by L in these complexes, the metal centres present different geometries. Both complexes and the ligand exhibit strong emission in the UV-Vis region. These luminescent compounds at room temperature presumably have potential usages in electro-optical devices [19–21].

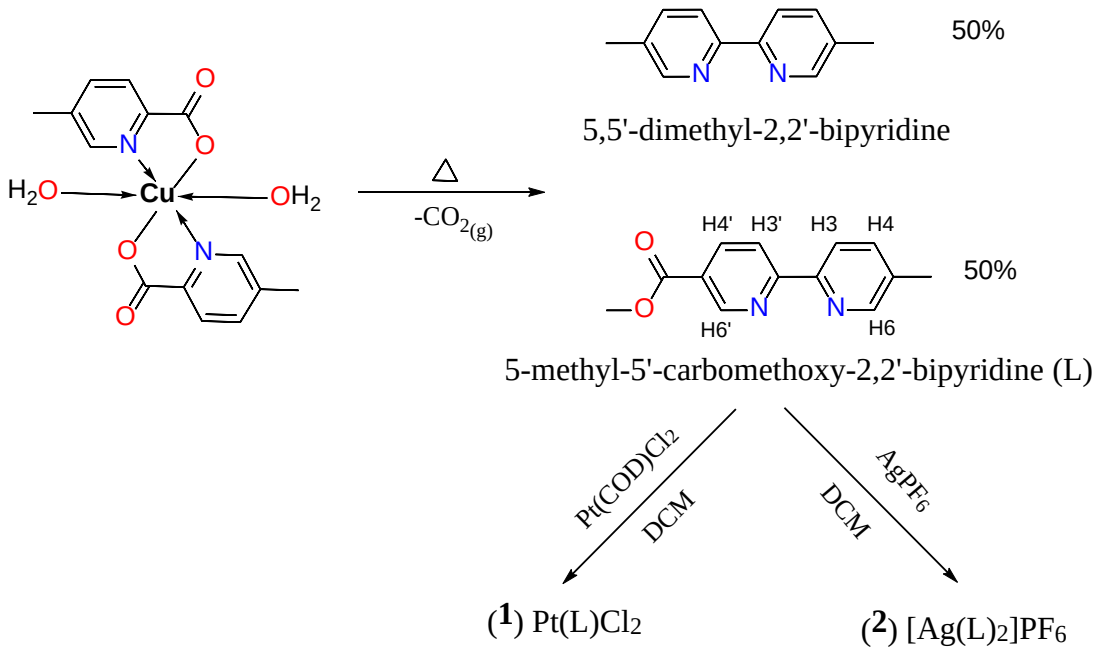

Scheme 1. Synthetic pathway for the compounds

2. Experimental

2.1. Materials and instruments

All chemicals were obtained from commercial sources and used without further purification unless otherwise stated. Elemental analysis data were performed on a LECO CHNS analyser (for C, H, N). ^{1}H NMR spectra were recorded on a Bruker DPX-400, 400 MHz High Performance Digital FT-NMR. Chemical shifts of ^{1}H is reported in parts per mil- lion (ppm) from tetramethylsilane (TMS). Chemical shifts are given in ppm relative to TMS as an internal standard in DMSO-d_6 as a solvent, the coupling constants J are given in Hz and spectra were recorded in parts per million (ppm). The IR spectra were recorded as ATR on a Perkin-Elmer FT-IR 100 spectrometer in the range of 4000-400 cm^{-1}. The APCI-MS mass studies were carried out on LC/MS Agilent 1100 MSD mass spectrometer. The ESI-MS studies were performed on a Thermo Finnigan LCQ Deca

quadrupole ion trap mass spectrometer (Thermo Finnigan, San Jose, CA). UV-Vis absorption spectra were performed at room temperature on a Carry VinUV 100 Bio, Varian spectrophotometer from the range of 200-600 nm, and the samples were in DMSO solution. Emission spectra at room temperature were collected in the wavelength range of 300–600 nm by using a Perkin Elmer LS55 Fluorescence Spectrometer.

2.2. Crystal structure determination

Single crystals of the compounds suitable for X-ray diffraction were grown from acetonitrile solution at room temperature by slow evaporation. The data was collected on a Bruker Nonius KappaCCD diffractometer with an Apex2 detector situated at the window of an FR591 rotating anode generator with Mo K_α radiation (λ = 0.71073 Å) selected by a confocal max-flux focusing mirror. The sample was kept at a temperature of 120(2) K. The lattice parameters were refined by least-squares based on all reflections with $F^2>2\sigma(F^2)$. Integration of intensities, correction for Lorentz and polarization effects, and cell refinements were performed using Bruker Nonius COLLECT software [22]. The structures were solved by direct methods using SHELXS-97 [23] and refined by a full-matrix least-squares procedure using the program SHELXL [24] within the Olex2 software package [25]. All hydrogen atoms were constrained to idealised positions and refined using a riding model. The PF_6 counter ion in **2** is disordered over two sites due to the symmetry of the space group (site ratio = 50:50). Details of crystal data, data collection, structure solution, and refinement for the structures of **1** and **2** are given in Table 1.

Table 1 Crystal data and structure refinement.

	1	**2**
Empirical formula	$C_{13}H_{12}Cl_2N_2O_2Pt$	$C_{26}H_{24}AgF_6N_4O_4P$
Formula weight	494.24	709.34
Temperature/K	120.15	120.15
Crystal system	monoclinic	monoclinic
Space group	$P2_1/c$	P2/c
a/Å	9.1229(2)	11.4692(4)
b/Å	17.9189(4)	8.1247(2)
c/Å	8.9761(2)	16.0726(4)
α/°	90	90
β/°	105.7300(10)	114.326(2)
γ/°	90	90
Volume/Å^3	1412.39(6)	1364.73(7)
Z	4	2
ρ_{calc}g/cm^3	23.241	17.260
μ/mm^{-1}	10.311	0.879
F(000)	923.4	710.9
Crystal size/mm^3	0.18 × 0.08 × 0.01	0.2 × 0.2 × 0.2
Radiation	Mo Kα (λ = 0.71073)	Mo Kα (λ = 0.71073)
2Θ range for data collection/°	6.08 to 55.1	7.32 to 55
Index ranges	$-11 \le h \le 11$, $-23 \le k \le 22$, $-11 \le l \le 10$	$-14 \le h \le 14$, $-10 \le k \le 10$, $-20 \le l \le 20$
Reflections collected	15268	16153
Independent reflections	3189 [R_{int} = 0.0383, R_{sigma} = 0.0314]	3131 [R_{int} = 0.0343, R_{sigma} = 0.0291]
Data/restraints/parameters	3189/0/178	3131/0/220
Goodness-of-fit on F^2	1.042	1.052
Final R indexes [I>=2σ (I)]	R_1 = 0.0385, wR_2 = 0.0914	R_1 = 0.0321, wR_2 = 0.0755
Final R indexes [all data]	R_1 = 0.0420, wR_2 = 0.0944	R_1 = 0.0366, wR_2 = 0.0780
Largest diff. peak/hole / e Å^{-3}	7.54/-1.20	0.70/-0.75

2.3. Computational details

Geometry optimizations in the gas phase and solution were performed using Gaussian09 software [26]. Gaussview 5.0 visual software [27] was used to obtain images for molecular structures, UV-Vis absorption spectra, and molecular orbitals of the investigated systems. Ground-state optimizations were carried out with Density Functional Theory (DFT) [28] using the hybrid B3LYP functional (B3: Becke's three-parameter nonlocal exchange functional [29, 30] LYP: Lee-Yang-Parr's correlation function [31]) together with the 6-311+G(d,p) basis set and with LANL2DZ basis set [32] (latter only for metals). Frequency analysis confirmed that the optimized structures are true minima. Calculations in solution were carried out using acetonitrile (ACN) and dimethylsulfoxide (DMSO) as solvents with the Polarizable Continuum Model (PCM) [33, 34]. The theoretical UV-Vis absorption spectra were obtained using the time-dependent DFT (TD-DFT) method at the same level as used in DFT optimizations to compare with the experimental UV-Vis absorption spectra. The first 80 singlet excited states for each system were used in vertical excitation calculations.

*2.4. Synthesis of 5-methyl-5'-carbomethoxy-2,2'-bipyridine (**L**)*

The preparation methods were previously reported for the analogous compound, 5,5′-dimethyl-2,2′-bipyrazine, in reference [35]. The ligand, 5-methyl-5'-carbomethoxy-2,2'-bipyridine was obtained by using the same synthetic method which yielded a mixture of two different products as revealed by the ^{1}H NMR studies. The pyrolysis of the copper(II) complex, *mono*-aqua-*bis*(*trans*-5-methyl-pyridine-2-carboxylato-*N*,*O*)copper(II) requires very high temperature, so the evolving gases may lead to react with the radicals of the reagent to yield a different product at such an elevated temperature and pressure in the reaction vessel. The precursor copper(II) complex was placed in a pyrolysis vessel

and heated at an elevated temperature until all of the product sublimed on the cold finger of the sublimation apparatus. The product was scratched and washed down into the beaker with acetone. The white precipitate was obtained by slow evaporation at room temperature.. The preliminary ^{1}H NMR investigation of the crude product showed that it is a (1:1) mixture of the symmetrically substituted 5,5′-dimethyl-2,2′-bipyridine and the unsymmetrically substituted 5-methyl-5′-carbomethoxy-2,2′-bipyridine (L) as shown in Scheme 1. The ligand was isolated from the mixture by column chromatography eluted with dichloromethane-hexane (1:1 v/v), and successive crystallisation from the solution yielded the pure product (~7%). m.p. 423 K. IR (ATR, υ/cm^{-1}): 3449sb, 3051w, 2951w, 2913vw, 1717 vs, 1597s, 1553m, 1469s, 1435s, 1372m, 1294vs, 1246w, 1219w, 1196m, 1115vs, 1054vw, 1029m, 960w, 844m, 813vw, 787m, 748m, 652m, 604vw, 506vw. ^{1}H-NMR (dmso-d_6, δ_{ppm}): 9.07 (s, 1H, H6'), 8.50 (d, J = 0.6 Hz 1H, H6), 8.41 (d, $J_{4',3'}$ = 8.3 Hz, 1H, H4'), 8.35 – 8.34 (m, 1H, H3'), 8.27 (d, $J_{3,4}$ = 8.1 Hz, 1H, H3), 7.73 (d, $J_{4,3}$ = 8.1 Hz, 1H, H4), 3.83 (s, 3H, OCH_3), 2.31 (s, 3H, CH_3). ^{13}C-NMR (dmso-d_6, δ_{ppm}): 165.9 (C=O), 159.5 (C2'), 152.5 (C2), 150.4 (C6'), 149.8 (C6), 137.9 (C4'), 137.6 (C4), 134.5 (C5'), 125.4 (C5), 121.5 (C3'), 120.3 (C3), 52.3 (OCH_3), 18.4 (CH_3). MS (APCI, m/z): 228.0 (100%) (L). Anal. Calc for $C_{13}H_{12}N_2O_2$: C, 68.41; H, 5.30; N, 12.27. Found: C, 68.31; H, 4.88; N, 11.96%.

*2.5. Synthesis of dichloro(5-methyl-5'-carbomethoxy-2,2'-bipyridine)platinum(II) (**1**)*

The ligand (0.010 g, 0.040 mmol) and Pt(COD)Cl_2 (0.032 g, 0.040 mmol) in 10 ml of DCM was set to reflux for 24 h. The resulting orange solution was evaporated to dryness. The crude product was dissolved in methanol and filtered to remove unreacted Pt(COD)Cl_2. The solid was recrystallized from acetonitrile to give orange crystals suitable for X-ray analysis. IR (KBr, υ/cm^{-1}): 3448sb, 3097vw, 3050w, 3007vw, 2955w,

2366vw, 2341vw, 1718vs, 1609m, 1475m, 1430s, 1380m, 1338w, 1306vs, 1276vs, 1191w, 1156m, 1130s, 1054w, 1009w, 954w, 906vw, 871w, 845m, 834m, 775m, 740m, 713vw, 695vw, 580vw, 474m, 416w. ^{1}H NMR (dmso-d_6, δ_{ppm}): 10.01 (d, $J_{6',4'}$ = 1.7 Hz, 1H, H6'), 9.34 (s, 1H, H6), 8.81 (dd, $J_{4',3'}$ = 8.4, $J_{4',6'}$ = 1.8 Hz, 1H, H4'), 8.66 (d, $J_{3',4'}$ = 8.5 Hz, 1H, H3'), 8.60 (d, $J_{3,4}$ = 8.3 Hz, 1H, H3), 8.31 (d, $J_{4,3}$ = 8.9 Hz, 1H, H4), 3.98 (s, 3H, OCH_3), 2.55 (s, 3H, CH_3). MS (APCI, m/z): 493.45 [M^+].

*2.6. Synthesis of bis(5-methyl-5'-carbomethoxy-2,2'-bipyridine)silver(I) hexafluorophosphate (**2**)*

A solution of L (0.031 g, 0.134 mmol) in DCM (20 cm^3) was treated with $AgPF_6$ (0.032 g, 0.126 mmol) in ACN (20 cm^3) under dry nitrogen in the dark (the reaction flask was covered with aluminium foil) and stirred at room temperature for 3h. The mixture was then set to reflux for 1h to yield a homogenous solution. After cooling down the solution to room temperature, the filtrate was allowed to stand at room temperature in the dark to afford amber colour crystals suitable for X-ray diffraction. 0.054 g (60%). IR (KBr, υ/cm^{-1}): 3047vw, 2951w, 2360m, 1717vs, 1653m, 1598m, 1558m, 1541m, 1507m, 1472m, 1436m, 1374m, 1294s, 1196w, 1115s, 1030w, 966vw, 844m, 787m, 747m, 652w, 517vw, 419w. ^{1}H NMR (dmso-d_6, δ_{ppm}): 9.20 (d, $J_{6',4'}$ = 1.5 Hz, 1H, H6'), 8.62 (s, 1H, H6), 8.56-8.51(m, 2H, H4' and H3'), 8.42 (d, $J_{3,4}$ = 8.2 Hz, 1H, H3), 7.94 (dd, $J_{4,3}$ = 8.2, $J_{4,6}$ =1.6 Hz, 1H, H4), 3.93 (s, 3H, OCH_3), 2.42 (s, 3H, CH_3). ^{13}C-NMR (dmso-d_6, δ_{ppm}): 165.3 (C=O), 157.9 (C2'), 152.1 (C2), 151.7 (C6'), 150.0 (C6), 138.9 (C4'), 138.5 (C4), 135.5 (C5'), 125.4 (C5), 122.1 (C3'), 120.9 (C3), 53.1 (OCH_3), 18.3 (CH_3). MS (ESI, m/z): 564.85 [AgL_2], 352.56 [$AgL+H_2O$]

3. Results and Discussion

*3.1. Spectroscopic characterization of L, **1**, and **2**.*

The ligand was obtained in low yield as described in the experimental part. The final product, 5-methyl-5'-carbomethoxy-2,2'-bipyridine (L) was characterized by mass spectrometry (Fig. S1), ^{1}H NMR (Fig. S2), ^{13}C NMR (Fig. S3), and ATR-IR (Fig. S4), respectively. The selected FT-IR data for L, **1** and **2** are collected in Table 2. The IR (Fig. S4) shows the characteristic bands for aromatic CH at 3051 cm^{-1} and aliphatic CH at 2951 cm^{-1}. The stretching band at 1717 cm^{-1} can easily be assigned to the C=O group. The ligand was fully characterized by ^{1}H NMR, in which the methyl and the carboxymethyl appeared at 2.31 and 3.83 ppm, respectively (Table 3). Thus, the presence of four singlet protons in the aromatic region (*vide supra*) confirms the structure. This was further supported by the ^{13}C NMR (Fig. S3), which shows as expected thirteen carbon atoms (see the experimental part for the assignment). Two of these are in the aliphatic region due to methyl resonance at 23.87 ppm and OCH_3 at 52.32 ppm, others are observed in the aromatic region as expected. The ligand was further characterized by mass spectrometry, where the molecular ion appeared at *m/z* 228.0, and confirms the molecular formula.

Table 2 Selected FT-IR spectral data for L, **1** and **2**.[a]

	L	**1**	**2**
υ(CH)	3051w	3050w	3047vw
υ(CH)	2951w	2955w	2951w
υ(CO)	1717vs	1718vs	1717vs
υ(CC, CN)	1597s,1552m,1469s, 1435s	1609m, 1475m, 1430s	1598s, 1558m,1472m, 1436s

[a] Frequencies in cm^{-1}. vs = very strong; s = strong; m = medium; w = weak; vw = very weak.

The platinum(II) complex (**1**) was also fully characterized. The IR spectrum (Fig. S5) is similar to that of the ligand (Table 2). In the ^{1}H NMR (Fig. S6), the corresponding methyl and methoxy groups appear at 2.53 and 3.98 ppm, respectively. These two signals show

very small downfield shifts compared to those of the free ligand (Table 3). However, the corresponding aromatic protons are significantly shifted downfield. This is clearly due to the coordination of the ligand to the platinum centre, which acts as a Lewis acid to withdraw electron density from the ligand. The molecular ion peak (Fig. S7) was observed in the mass spectrum at *m/z* 493.4 [M^+] (calculated for $C_{13}H_{12}N_2O_2Cl_2Pt$ *m/z* = 493.9), identical to the theoretical value calculated for the molecular structure. This peak can be detected in the mass data but is absent in the spectrum range due to the chemical ionization method, which afforded a highly fragmented spectrum. In the spectrum, the defragmented ligand and the $PtCl_2$ moieties can be easily noticed at *m/z* = 227.0 and 265.2, respectively. The complex was also characterized by single-crystal X-ray diffraction (*vide infra*).

Coordination of a silver(I) ion with the ligand surprisingly afforded a mononuclear cationic complex (**2**), which was also characterized by IR, ^{1}H NMR, and mass spectrometry. The IR spectrum (Fig. S8) is very similar to that of the ligand (Table 2). In the ^{1}H NMR (Fig. S9) the methyl and methoxy group are observed as a singlet at 2.4 and 3.9 ppm, respectively. The corresponding four aromatic protons have a resonance between 9.2 and 8.3 ppm, showing almost the same pattern of the free ligand with an insignificant downfield shift (Table 3).

Table 3 ^{1}H NMR chemical shifts (with respect to TMS) for L, **1** and **2** in DMSO-d_6.[a]

	H6'	H6	H4'	H3'	H3	H4	OCH_3	CH_3
L	9.07(s)	8.50(d)	8.41(d)	8.35-8.34(m)	8.27(d)	7.73(d)	3.83(s)	2.31(s)
1	10.01(d)	9.34(s)	8.81(dd)	8.66(d)	8.60(d)	8.31(d)	3.98(s)	2.55(s)
2	9.20(d)	8.62(s)	8.56-8.51(m)		8.42(d)	7.94(dd)	3.93(s)	2.42(s)

[a] s = singlet; d = doublet; dd = doublet of doublet; m = multiplet.

The complex (**2**) was further characterized by mass spectrometry (Fig. S10), in which the molecular ion peak was observed at *m/z* 564.7 (calculated for $C_{26}H_{24}N_4O_4Ag$ *m/z* = 564.0) which is consistent with the theoretical molecular weight of the cation $[Ag(L)_2]^+$.

The UV-Vis and luminescence spectra of L, **1**, and **2** were measured in DMSO at room temperature (Fig. 1) and the data are listed in Table 4. The ligand displays a very strong absorption band at 307 nm that is assigned to π→π* transitions. The UV-Vis spectrum of **2** displays π→π* transitions at 301 nm with similar vibrational progression but undergoes a blue shift, while in that of **1** the high energy band at 265 nm is very intense, having shoulder at around 300 nm which is more pronounced and comparatively blue-shifted. In **1**, significantly low energy absorption bands observed at around 328-338 nm and a weak absorption band at 400 nm are assigned to a combined metal-to-ligand (ML) and intra-ligand (IL) charge transfer (CT) transitions [36].

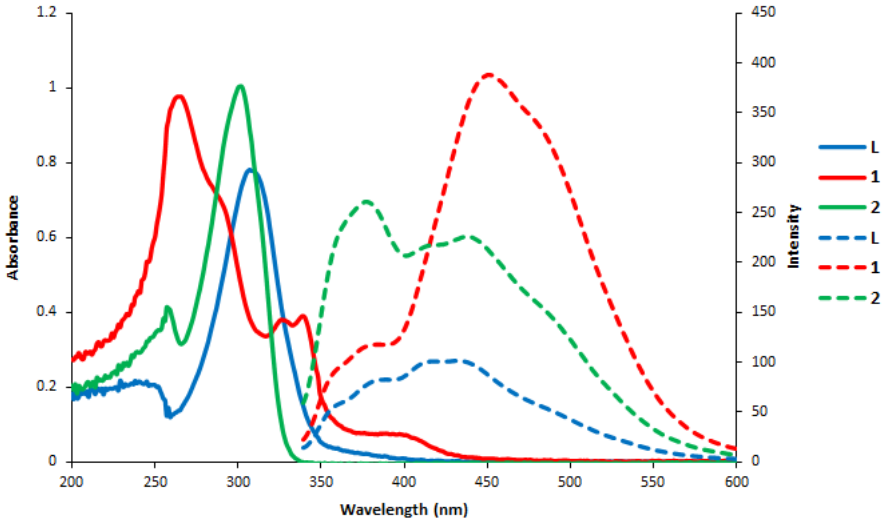

Fig. 1. UV–Vis absorption and fluorescence emission of L, **1,** and **2** in DMSO. (solid line: electronic absorption, dashed line: fluorescence emission).

The ligand and the corresponding metal complexes are luminescent in DMSO solution at room temperature. The emission maxima data are summarised in Table 4. The emission energies of the ligand and the complexes parallel the shifts observed in the absorption spectra. Interestingly, all compounds have very similar emission spectra (Fig. 1). The intensity of the emissions decreases in the order **1** > **2** > L as shown in Fig. 1. The enhancement of the luminescence of the metal complexes may be attributed to the ligation of L to the metal centres, which effectively increases the rigidity of the ligand and reduces the loss of energy by radiation-less decay [37, 38]. On the other hand, the emission bands centred between 380 and 600 nm for all compounds, the platinum(II) complex (**1**) exhibits the most red-shifted emission ($\lambda_{max} \approx 450$ nm), while that of the silver(I) (**2**) and L are very similar. Their emissions seem to originate mainly from $\pi \rightarrow \pi^*$ (L) intra-ligand (IL) excited states.

Table 4 UV–Vis absorption and fluorescence emission of L, **1,** and **2** in DMSO.

Compound	λ_{abs}, nm	λ_{ex}, nm	λ_{em}, nm
L	245, 307	320	384.5, 431.5
1	265, 329, 338	350	380.5, 449.5
2	257, 301	310	378.5, 441.5

3.2. Structural analyses

The details of the crystal data collection and refinement of complexes **1** and **2** are summarized in Table 1. Selected bond distances and angles for both metal complexes are collected in Table 5. A thermal ellipsoid plot of **1** with the atom numbering scheme as shown in Fig. 2, indicates that the Pt(II) ion exhibits a square-planar geometry, completed by two nitrogen atoms from the chelating ligand L, (through the N1 and N2 positions)

and two chloride ligands. The platinum atom in **1** deviates by 0.67(7) Å from the best plane of the PtN_2Cl_2 chromophore. There is a small distortion from the ideal square planar geometry, as revealed by the narrowing of the N2–Pt1–N1 angle to 80.4(2)°, similar to analogous compounds [39, 40]. The mean plane of the chromophore PtN_2Cl_2 makes angles with the ligand rings, namely [N2-C13-C10-C9-C8-C7] and [N1-C6-C5-C4-C2-C1], 8.71 (4) and 9.03(4)°, respectively. The torsion angle, N2-C7-C6-N1 1.32(5)° shows a deviation of the pyridine rings from the planarity, as observed in the $Pt(bpy)Cl_2$ [41]. The deviation from ideal square planar geometry may be due to C–H···Cl interactions between the coordinated chloride ligands and the hydrogen atoms of L (Fig. 3). These interactions form a linear chain along the *c*-axis, while a 2-dimensional zig-zag layer is generated along the b axis via C–H···O hydrogen bonds (Fig. 3). The overall packing is stabilized by weak C–H···Cl interactions [42]. The molecules are stacked in a head-to-tail fashion akin to the related platinum(II) complexes with terpy ligands [40,43–46]. The Pt···Pt separation of 3.509 Å again reflects similarity with those of platinum(II) complexes and indicates the intermolecular π-π interactions [40]. As shown by the previous investigations on the platinum(II) linear-chain systems, their electronic and photoluminescence properties strongly depend on the intra-chain metal separation [45]. The Pt–N bond distances of 2.007(6) and 2.004(6)Å, and the Pt–Cl bond distances of 2.299(1) and 2.305(5)Å are in the expected range and can be compared to those of the related platinum(II) complexes in the literature [39, 47, 48].

Table 5 Selected bond lengths [Å] and angles [°].

			1			
Pt1	Cl2	2.3053(17)	Cl1	Pt1	Cl2	89.53(6)
Pt1	Cl1	2.2985(17)	N1	Pt1	Cl2	174.81(17)
Pt1	N1	2.008(6)	N1	Pt1	Cl1	95.13(17)
Pt1	N2	2.004(6)	N2	Pt1	Cl2	94.91(17)
N1	C6	1.357(9)	N2	Pt1	Cl1	175.32(17)
N1	C1	1.345(9)	N2	Pt1	N1	80.4(2)
C13	C10	1.398(10)	C6	N1	Pt1	115.2(5)
C13	N2	1.337(9)	C1	N1	Pt1	125.4(5)
C5	C6	1.384(10)	C1	N1	C6	119.4(6)
C5	C4	1.405(10)	N2	C13	C10	122.3(6)
C6	C7	1.474(9)	C5	C6	N1	121.4(6)
C2	C1	1.394(10)	C7	C6	N1	114.3(6)
C2	C4	1.373(10)	C2	C1	N1	122.5(6)
C2	C3	1.511(11)	N2	C7	C6	114.2(6)
C10	C9	1.396(10)	N2	C7	C8	121.8(6)
C10	C11	1.492(10)	C12	O1	C11	115.5(6)
C9	C8	1.386(10)	O1	C11	C10	111.5(6)
C8	C7	1.383(9)	O2	C11	C10	123.1(7)
C7	N2	1.359(9)	O2	C11	O1	125.5(7)
O1	C11	1.317(9)	C13	N2	Pt1	125.7(5)
O1	C12	1.461(9)	C7	N2	Pt1	115.3(4)
O2	C11	1.193(9)	C7	N2	C13	118.9(6)
			2			
Ag1	N1	2.2541(17)	N11	Ag1	N1	140.42(9)
Ag1	N11	2.2541(17)	N21	Ag1	N1	141.15(7)
Ag1	N21	2.4060(19)	N2	Ag1	N1	71.47(7)
Ag1	N2	2.4060(19)	N21	Ag1	N11	71.47(7)
O1	C12	1.203(3)	N2	Ag1	N11	141.15(7)
O2	C12	1.337(3)	N21	Ag1	N2	94.15(9)
O2	C13	1.449(3)	C13	O2	C12	115.23(18)
N1	C1	1.343(3)	C1	N1	Ag1	121.28(14)
N1	C6	1.346(3)	C6	N1	Ag1	119.51(14)
C4	C2	1.386(3)	C6	N1	C1	119.18(18)
C4	C5	1.380(4)	C7	N2	Ag1	114.42(14)
N2	C7	1.348(3)	C11	N2	Ag1	126.84(15)
N2	C11	1.332(3)	C11	N2	C7	118.64(19)
C9	C8	1.380(3)	C2	C1	N1	123.8(2)
C9	C10	1.384(3)	C5	C6	N1	120.3(2)
C1	C2	1.391(3)	C7	C6	N1	117.46(18)
C2	C3	1.504(3)	C6	C7	N2	117.12(19)
C5	C6	1.396(3)	C8	C7	N2	121.1(2)
C6	C7	1.489(3)	C10	C11	N2	123.6(2)
C7	C8	1.393(3)	O2	C12	O1	124.2(2)
C10	C11	1.386(3)	C10	C12	O1	124.2(2)
C10	C12	1.494(3)	C10	C12	O2	111.62(18)

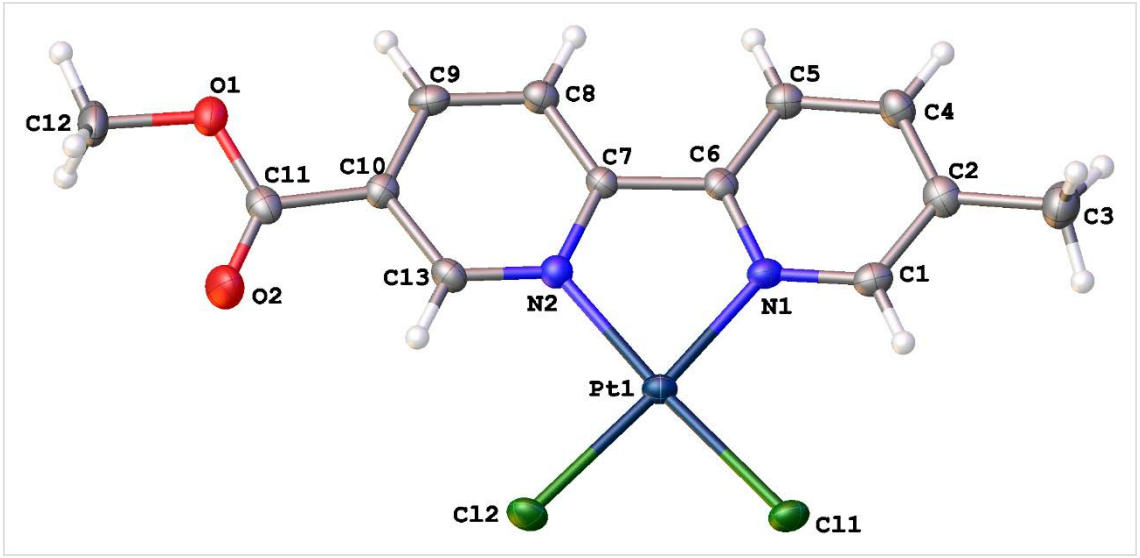

306

307 **Fig. 2.** Molecular structure of **1** with the atom labeling scheme.

308

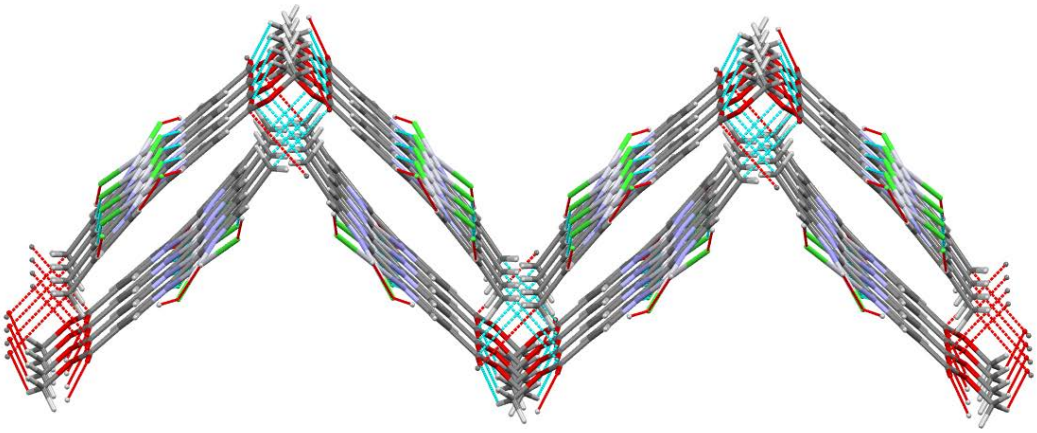

309

310 **Fig. 3.** The packing and significant intermolecular interactions formed in the structure of

311 **1**.

312 A perspective view of **2** is shown in Fig. 4. The asymmetric unit of **2** is built up of an

313 $[Ag(L)_2]^+$ cation and a PF_6 anion. In the cation, the silver(I) ion is coordinated by two

314 ligands through the nitrogen atoms in a chelating fashion to form an MN_4 chromophore.

315 The coordination around the Ag(I) ion can be best described as a flattened tetrahedron

316 geometry as depicted in Fig.4. The four Ag–N bond distances in **2** show a disparity with

two short [2.254(4) Å for Ag–N(1)] and two long [2.406(5) Å for Ag-N(3)] bonds and agree with those reported in the literature [49, 50]. The N–Ag–N bite angles for the chelate ring(s) have an average value of 61.68°. The angle between the two mean planes for each ligand is 50.93°. A torsion angle of 90° is expected for a perfect tetrahedron, whereas a torsion angle of 0° is expected for a square-planar arrangement. Thus, the present case can be best described as a flattened tetrahedron. The pyridine rings in the chelating ligands are almost coplanar with an insignificant deviation of 3.41° from the mean plane, as expected from the analogous ligand system [43].

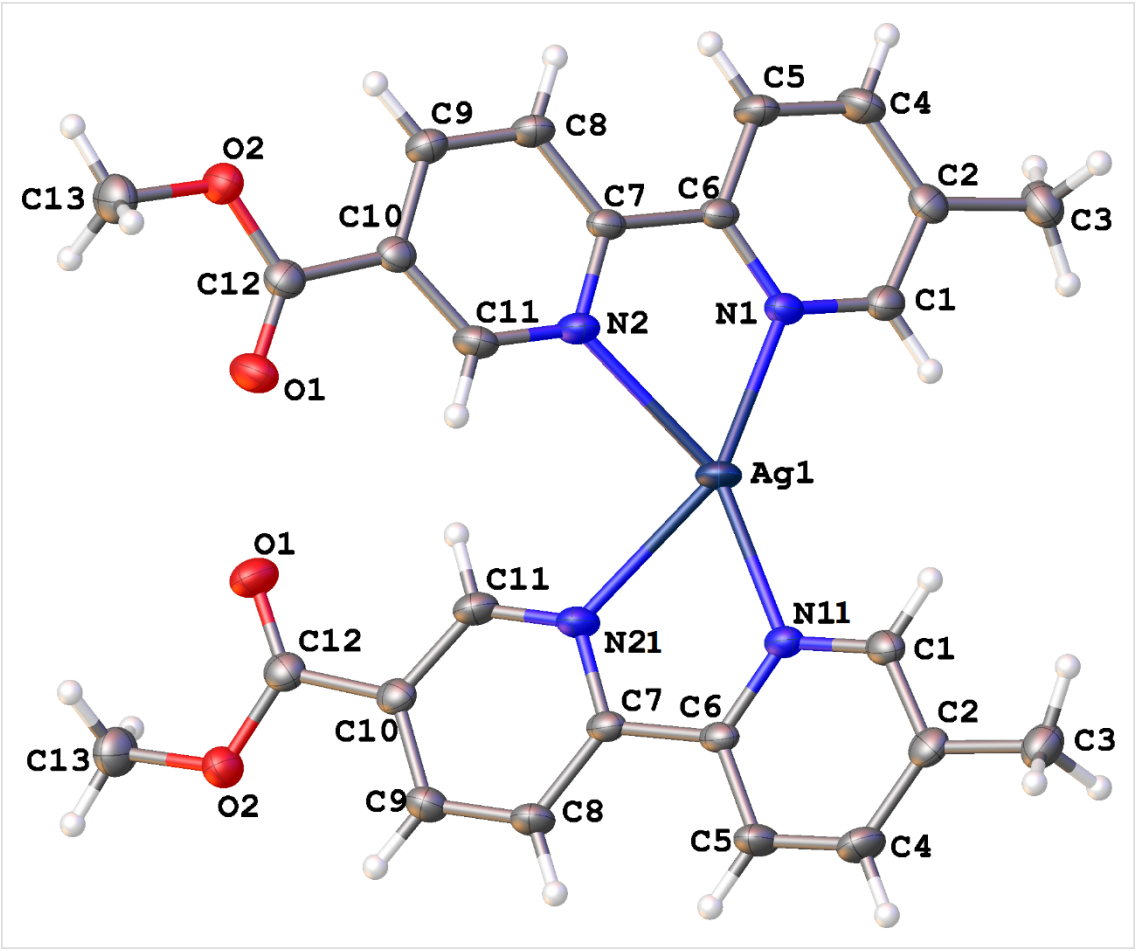

Fig. 4. Molecular structure of **2** with the atom labeling scheme.The ~~PF_6~~ counter ion was omitted for clarity.

329

330 *3.3. Computational results*

331 The ground-state, gas-phase optimized structures of **1** and **2** for ACN and DMSO
332 are given in Fig. S11 at the B3LYP/6-311+G(d,p) level with a LANL2DZ basis set on the
333 metals. Compound **1** has a planar geometry, however, the 2,2'-bipyridine ligands almost
334 form a perpendicular angle (O1-Ag-O1: 82.97° in the gas phase, 86.99° in DMSO) in
335 compound **2**. Additionally, the Pt centre is square-planar whereas the Ag centre adopts a
336 distorted tetrahedral structure. The experimental and the calculated bond distances and
337 bond angles are listed in Table S1 and Table S2 for comparison. Figures S12 and S13
338 provide a better overall understanding of all the differences in distances and angles. The
339 experimental and calculated values are generally similar for planar compound **1**.
340 However, the Ag-N distance is slightly larger in both gas phase and solution compared to
341 the crystal structure in compound **2**.

342 As for the angles, the largest difference (deviation) between the experimental and
343 the computational values is 32.95° measured for the N21-Ag1-N2 bond angle in DMSO.
344 The dihedral angle between pyridine rings is nearly 10.87° in the gas phase and 13.01° in
345 DMSO (N2-C7-C6-C5). It is highly probable that these differences are a result of a more
346 dense and compact structure in the crystal form due to the presence of neighbouring
347 molecules and the attractive interaction between them compared to the single molecules
348 used for the calculations in the gas phase and solution.

349 Some of the selected parameters of the molecule calculated with the B3LYP
350 functional, including the sum of electronic energies with thermal free energies ($E_{elec}+\Delta G$)
351 and total electronic energies with zero-point energy corrections (E_{elec}+ZPE, Hartree) in
352 the gas phase and solvents are given in Table S3. When the dielectric constant of the

medium is increased, the dipole moment of the molecule is also increased and the molecule is more stable at room temperature (negative ΔE and ΔΔG).

The frontier molecular orbitals and energy gaps of **1** and **2** in DMSO were shown in Fig. 5. As seen from the figure, the HOMO and LUMO are localized in different parts of the molecules. While the HOMO is localized mostly on the chlorine and Pt atoms, the LUMO is localized on π-antibonding orbitals in compound **1**. The HOMO is localized on the d orbitals of Ag and nonbonding electrons on N for compound **2**. The LUMO is also localized on the bpy rings as in compound **1**. The value of the energy separation between the HOMO and LUMO is 2.64 eV and 4.31 eV for **1** and **2** respectively.

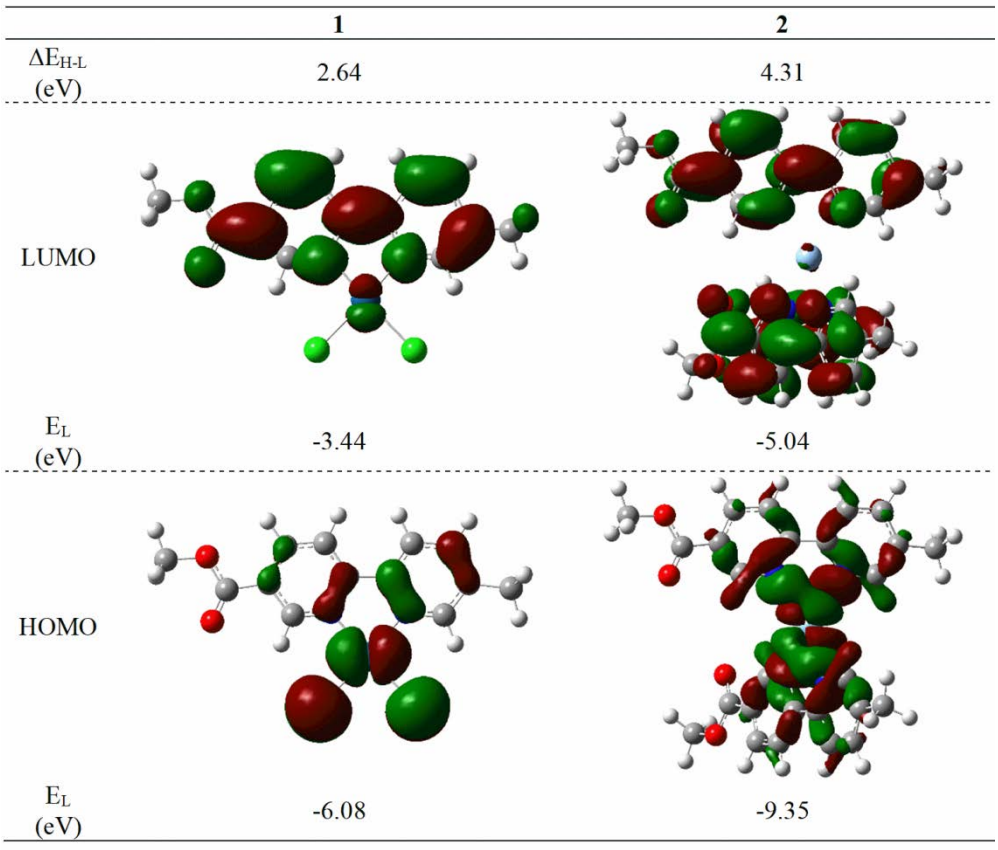

Fig. 5. Frontier orbital energies (E_H, E_L) and energy gaps (ΔE_{H-L}) of investigated compounds at B3LYP/6-311+G(d,p)/LANL2DZ level in DMSO (orbitals were

366 generated using Gaussview with an isovalue of 0.02)

367

368 The B3LYP/6-311+G(d,p)/LANL2DZ level was used in TD-DFT calculations to
369 obtain the absorption wavelengths and excitation energies for the first 80 singlet excited
370 states (from S_0 to S_{80}). Fig. S14 shows the calculated UV-Vis absorption spectrum for **1**
371 in DMSO. The selected electronic transitions and the corresponding orbitals for the
372 compound are displayed in Table S4 and Fig. S15 respectively.

373 There are three charge transfer types observed for compound **1**: metal-to-ligand
374 charge transfer (MLCT), ligand-to-metal charge transfer (LMCT), and charge transfer
375 from the chlorine atoms to the pyridine rings (CT). The $S_0 \rightarrow S_3$ transition (405 nm) has
376 intramolecular charge transfer from the chlorine atoms to the bpy rings between the
377 HOMO-2 and the LUMO orbitals. Additionally, it has MLCT from the Pt to the bpy rings
378 (MLCT1). It appears approximately at 400 nm in experimental spectrum.

379 The maximum oscillator strength peak at 329.5 nm displays a local excitation of
380 bpy rings (LE3) with π-π* character (Fig. S14, experimental peak value is 265 nm). The
381 transition at 302 nm has LE3 between the HOMO-2 and the LUMO+2. The S_{13} transition
382 has also CT1 and MLCT1 at 302 nm. In the calculated spectrum, there is an additional
383 absorption at 277 nm, which has the transition from the HOMO-5 of chlorine atoms to
384 the LUMO+2 of d orbitals on Pt (LMCT2: ligand-to-metal charge transfer). The S_{19}
385 transition displays local excitation for chlorine atoms (LE2) at 277 nm. At wavelengths
386 below 250 nm, π-π* character of the absorption peaks for the local excitation for bpy ring
387 (LE3) causes a slight increase in oscillator strength.

388 Fig. S16 shows the calculated UV-Vis absorption spectrum for compound **2** in
389 DMSO. The selected electronic transitions and the corresponding orbitals for the

compound are displayed in Table S5 and Fig. S17 respectively. Unlike **1**, the electronic transitions for **2** are mostly concentrated on MLCT from Ag to bpy rings (MLCT1). The S_1 transition at 382.5 nm mainly consists of MLCT1 character from the highest occupied molecular orbital (HOMO Ag) to the lowest unoccupied molecular orbital of the bpy rings (LUMO bipyridine). However, it is not observed in the experimental results because of its weak osciallator strength. The maximum peak at 318.4 nm displays a π-π* transition from the HOMO-2 of the bpy to the LUMO of the bpy rings. It is consistent with 307 nm in experimental spectrum. Both MLCT1 and local excitation of bpy (LE2) were observed at wavelengths below 269 nm.

The molecular electrostatic potential relates to the electronic density and also emphasizes its molecular shape, charge distribution, and the positive, negative, and zero electrostatic potential regions. MEPS analysis enables the identification of electron donor and electron acceptor regions that are particularly useful for understanding intramolecular and intermolecular interactions. Such visual analysis for intermolecular interactions is consistent with those revealed by X-ray diffraction analysis. MEP was obtained at the B3LYP/6-311+G(d,p)/LANL2DZ level to investigate the nucleophilic or electrophilic region of the molecules examined. Fig. 6 shows the MEPS of **1** and **2** in DMSO (mapped in the range between -0.116 au and +0.116 a.u. for **1**; between -0.124 au and +0.124 a.u. for **2**). The total electron density was calculated using the Mulliken charge distribution. Different colours refer to different values of the electrostatic potentials. The negative charges are mostly localized on the electronegative Cl atoms as expected. Therefore, the electrophilic attack can occur through Cl atoms. On the other hand, compound **2** has mostly positively charged regions. Therefore, it is more susceptible to nucleophilic attack by other species.

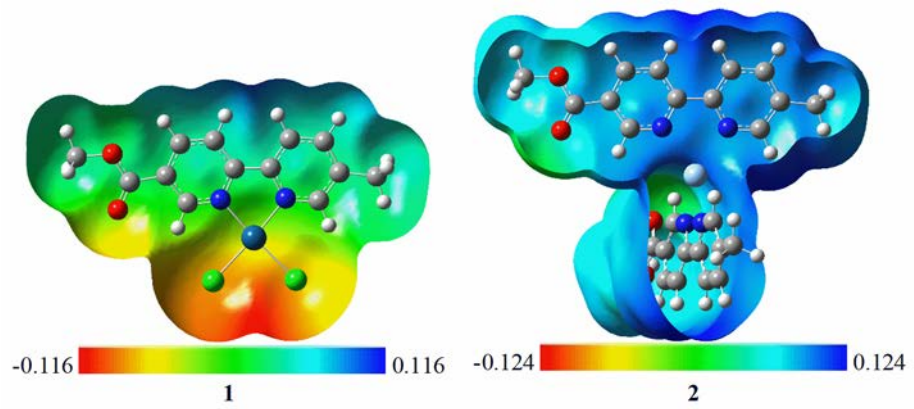

Fig. 6. Map of the molecular electrostatic potential surface for compounds **1** and **2** in DMSO calculated at B3LYP/6-311+G(d,p)/LANL2DZ level. Colours represent electron density: red, electron-rich; yellow, slightly electron-rich region; green, neutral; light blue, slight electron deficiency; blue, electron deficiency; isovalue is 0.02.

4. Conclusion

This paper reports on, for the first time, the synthesis and characterization of unsymmetrically substituted 5-methyl-5'-carbomethoxy-2,2'-bipyridine (L) and also preparation and single-crystal X-ray structures of its metal complexes with silver(I) and platinum(II). All the compounds are luminescent at room temperature and display low energy emission, which is very important for optoelectronic applications. Experimental and calculated structures have similar geometries. Calculated UV-Vis absorption spectra show that **2** has more MLCT than **1**. However, compound **1**, carrying a highly electronegative Cl atom, displays different charge transfers with both Pt and bpy; additionally, it shows absorption bands at longer wavelengths than 400 nm because of its

smaller HOMO-LUMO energy gap. Molecular electrostatic potential calculations revealed that **1** has a nucleophilic nature whereas **2** behaves as an electrophile.

Acknowledgments

The authors are grateful to the Turkish Scientific and Technical Research Council [TBAG-2450 (104T060)] and also Zonguldak Bülent Ecevit University for grant 2007/3-13-02-01. The authors also wish to acknowledge the UK Engineering and Physical Sciences Research Council for funding the National Crystallography Service. Computer time provided by Fen Cluster (Ege University Faculty of Science) and TUBITAK ULAKBIM TRUBA Resources is gratefully acknowledged.

Supplementary data

Crystallographic data for the structural analysis of **1** and **2** have been deposited with the Cambridge Crystallographic Data Centre, CCDC 1812726, and CCDC 1812727, respectively. Copies of this information may be obtained free of charge from the Director, CCDC, 12 Union Road, Cambridge, CB2 1EZ, UK (fax: +44-1223-336033; e-mail: deposit@ccdc.cam.ac.uk or http://www.ccdc.cam.ac.uk/deposit).

References

[1] C. Seward, J. Chan, D. Song, S. Wang, Anion Dependent Structures of Luminescent Silver(I) Complexes, Inorg. Chem. 42 (2003) 1112–1120. http/doi.org/10.1021/ic020480q.

[2] D. Paul Rillema, A.J. Cruz, C. Moore, K. Siam, A. Jehan, D. Base, T. Nguyen, W.

453 Huang, Electronic and Photophysical Properties of Platinum(II) Biphenyl
454 Complexes Containing 2,2′-Bipyridine and 1,10-Phenanthroline Ligands, Inorg.
455 Chem. 52 (2012) 596–607. http/doi.org/10.1021/ic301393e.

456 [3] L.J. Grove, J.M. Rennekamp, H. Jude, W.B. Connick, A New Class of Platinum(II)
457 Vapochromic Salts, J. Am. Chem. Soc. 126 (2004) 1594–1595.
458 http/doi.org/10.1021/ja037783j.

459 [4] T.J. Wadas, Q.-M. Wang, Y. Kim, C. Flaschenreim, T. N. Blanton, R. Eisenberg,
460 Vapochromism and Its Structural Basis in a Luminescent Pt(II)
461 Terpyridine−Nicotinamide Complex, J. Am. Chem. Soc. 126 (2004) 16841–16849.
462 http/doi.org/10.1021/ja047955s.

463 [5] C. Cebrián, M. Mauro, D. Kourkoulos, P. Mercandelli, D. Hertel, K. Meerholz,
464 C.A. Strassert, L. De Cola, Luminescent Neutral Platinum Complexes Bearing an
465 Asymmetric N^N^N Ligand for High-Performance Solution-Processed OLEDs,
466 Adv. Mater. 25 (2013) 437–442. http/doi.org/10.1002/adma.201202123.

467 [6] S.C.F. Kui, F.-F. Hung, S.-L. Lai, M.-Y. Yuen, C.-C. Kwok, K.-H. Low, S.S.-Y.
468 Chui, C.-M. Che, Luminescent Organoplatinum(II) Complexes with Functionalized
469 Cyclometalated C^N^C Ligands: Structures, Photophysical Properties, and
470 Material Applications, Chem. – A Eur. J. 18 (2012) 96–109.
471 http/doi.org/10.1002/chem.201101880.

472 [7] T.-T. Yeh, J.-Y. Wu, Y.-S. Wen, Y.-H. Liu, J. Twu, Y.-T. Tao, K.-L. Lu,
473 Luminescent silver metal chains with unusual μ4-bonded 2,2′-bipyrazine, Dalt.
474 Trans. (2005) 656–658. http/doi.org/10.1039/B416703A.

[8] D.N. Kozhevnikov, O. V. Shabunina, D.S. Kopchuk, P.A. Slepukhin, V.N. Kozhevnikov, 5-Aryl-2,2′-bipyridines as tunable fluorophores, Tetrahedron Lett. 47 (2006) 7025–7029. http/doi.org/10.1016/J.TETLET.2006.07.111.

[9] R. Bodapati, M. Sarma, A. Kanakati, S. K. Das, Asymmetrically Substituted and π-Conjugated 2,2′-Bipyridine Derivatives: Synthesis, Spectroscopy, Computation, and Crystallography, J. Org. Chem. 80 (2015) 12482–12491. http/doi.org/10.1021/acs.joc.5b02345.

[10] S. Mazzucato, I. Fortunati, S. Scolaro, M. Zerbetto, C. Ferrante, R. Signorini, D. Pedron, R. Bozio, D. Locatelli, S. Righetto, D. Roberto, R. Ugo, A. Abbotto, G. Archetti, L. Beverina, S. Ghezzi, Two-photon absorption of Zn(ii) octupolar molecules, Phys. Chem. Chem. Phys. 9 (2007) 2999–3005. http/doi.org/10.1039/B618709A.

[11] C. Kaes, A. Katz, M. Wais Hosseini, Bipyridine: The Most Widely Used Ligand. A Review of Molecules Comprising at Least Two 2,2‘-Bipyridine Units, Chem. Rev. 100 (2000) 3553–3590. http/doi.org/10.1021/cr990376z.

[12] H. Le Bozec, T. Renouard, Dipolar and Non-Dipolar Pyridine and Bipyridine Metal Complexes for Nonlinear Optics, Eur. J. Inorg. Chem. 2000 (2000) 229–239. http/doi.org/10.1002/(SICI)1099-0682(200002)2000:2<229::AID-EJIC229>3.0.CO;2-A.

[13] A.G. Young, L.R. Hanton, Square planar silver(I) complexes: A rare but increasingly observed stereochemistry for silver(I), Coord. Chem. Rev. 252 (2008) 1346–1386. doi:10.1016/J.CCR.2007.07.017.

[14] C.-J. Wang, Y.-Y. Wang, H. Wang, G.-P. Yang, G.-L. Wen, M. Zhang, Q.-Z. Shi, A novel silver(I) coordination polymer based on mixed ligands bpp and 2,2′-bipyridine-4,4′-dicarboxylate, Inorg. Chem. Commun. 11 (2008) 843–846. http/doi.org/10.1016/J.INOCHE.2008.04.013.

[15] A. Kraft, A.C. Grimsdale, A.B. Holmes, Electroluminescent Conjugated Polymers—Seeing Polymers in a New Light, Angew. Chemie Int. Ed. 37 (1998) 402–428. http/doi.org/10.1002/(SICI)1521-3773(19980302)37:4<402::AID-ANIE402>3.0.CO;2-9.

[16] V. M. Miskowski, V. H. Houlding, C. Ming Che, Y. Wang, Electronic spectra and photophysics of platinum(II) complexes with .alpha.-diimine ligands. Mixed complexes with halide ligands, Inorg. Chem. 32 (2002) 2518–2524. http/doi.org/10.1021/ic00063a052.

[17] J.A. Gareth Williams, S. Develay, D.L. Rochester, L. Murphy, Optimising the luminescence of platinum(II) complexes and their application in organic light emitting devices (OLEDs), Coord. Chem. Rev. 252 (2008) 2596–2611. http/doi.org/10.1016/J.CCR.2008.03.014.

[18] J. Ni, Y.-G. Wang, H.-H. Wang, Y.-Z. Pan, L. Xu, Y.-Q. Zhao, X.-Y. Liu, J.-J. Zhang, Reversible Dual-Stimulus-Responsive Luminescence and Color Switch of a Platinum Complex with 4-[(2-Trimethylsilyl)ethynyl]-2,2′-bipyridine, Eur. J. Inorg. Chem. 2014 (2014) 986–993. http/doi.org/10.1002/ejic.201301329.

[19] J. Zyss, Molecular nonlinear optics: materials, physics, and devices, Academic press, 2013.

[20] S-Z. Zhan, F. Ding, X-W. Liu, G-H. Zhang, J. Zheng, D. Li, White Light from Blue Fluorescence and Sensitized Yellow Long-Afterglow Phosphorescence of o-Terphenyl in Its π-Acid···Base Adduct with Ag3Pz3, Inorg. Chem. 58 (2019) 19, 12516–12520. https://doi.org/10.1021/acs.inorgchem.9b01911

[21] S-Z. Zhan, W. Chen, W. Lu, J. Zheng, F. Ding, T. Feng, D. Li, Counteranion-Triggered and Excitation-Dependent Chemopalette Effect in a Supramolecular Dual-Emissive System Based on Cu_3Pz_3, Inorg. Chem. 58 (2019) 2, 1081–1090. https://doi.org/10.1021/acs.inorgchem.8b02203

[22] B. V Nonius, Collect software, Nonius, Delft, The Netherlands. (1998).

[23] G.M. Sheldrick, SHELXT− Integrated Space-Group and Crystal-Structure Determination, Acta Crystallogr., Sect. C Struct. Chem. 71 (2015) 3–8.

[24] G.M. Sheldrick, Crystal structure refinement with SHELXL, Acta Crystallogr., Sect. C Struct. Chem. 71 (2015) 3-8.

[25] O.V. Dolomanov, L.J. Bourhis, R.J. Gildea, J.A.K. Howard, H. Puschmann (2009). OLEX2 J Appl Cryst 42:339

[26] M.J. Frisch, G.W. Trucks, H.B. Schlegel, G.E. Scuseria, M.A. Robb, J.R. Cheeseman, G. Scalmani, V. Barone, B. Mennucci, G.A. Petersson, H. Nakatsuji, M. Caricato, X. Li, H.P. Hratchian, A.F. Izmaylov, J. Bloino, G. Zheng, J.L. Sonnenberg, M. Hada, M. Ehara, K. Toyota, R. Fukuda, J. Hasegawa, M. Ishida, T. Nakajima, Y. Honda, O. Kitao, H. Nakai, T. Vreven, J.A. Montgomery, Jr., J.E. Peralta, F. Ogliaro, M. Bearpark, J.J. Heyd, E. Brothers, K.N. Kudin, V.N. Staroverov, R. Kobayashi, J. Normand, K. Raghavachari, A. Rendell, J.C. Burant,

S.S. Iyengar, J. Tomasi, M. Cossi, N. Rega, J.M. Millam, M. Klene, J.E. Knox, J.B. Cross, V. Bakken, C. Adamo, J. Jaramillo, R. Gomperts, R.E. Stratmann, O. Yazyev, A.J. Austin, R. Cammi, C. Pomelli, J.W. Ochterski, R.L. Martin, K. Morokuma, V.G. Zakrzewski, G.A. Voth, P. Salvador, J.J. Dannenberg, S. Dapprich, A.D. Daniels, Ö. Farkas, J.B. Foresman, J.V. Ortiz, J. Cioslowski and D.J. Fox, Gaussian 09 C.01, Gaussian, Inc. Wallingford CT. (2009).

[27] R.D. Dennington, T.A. Keith, J.M. Millam, others, GaussView 5.0. 8, Gaussian Inc. 340 (2008).

[28] W. Kohn, L.J. Sham, Self-consistent equations including exchange and correlation effects, Phys. Rev. 140 (1965) A1133-A1138. http/doi.org/ 10.1103/PhysRev.140.A1133

[29] A.D. Becke, Density-functional exchange-energy approximation with correct asymptotic behavior, Phys. Rev. A. 38 (1988) 3098-3100. http/doi.org/ 10.1103/PhysRevA.38.3098

[30] A.D. Becke, Becke's three parameter hybrid method using the LYP correlation functional, J. Chem. Phys. 98 (1993) 5648–5652. http/doi.org/10.1063/1.464913

[31] C. Lee, W. Yang, R.G. Parr, Development of the Colle-Salvetti correlation-energy formula into a functional of the electron density, Phys. Rev. B. 37 (1988) 785-789. http/doi.org/10.1103/PhysRevB.37.785

[32] T.H. Dunning, P.J. Hay, Methods of electronic structure theory, in: Mod. Theor. Chem., Plenum Press New York, 1977: p. 1-28. http/doi.org/10.1007/978-1-4757-0887-5_1.

[33] J. Tomasi, B. Mennucci, E. Cances, The IEF version of the PCM solvation method: an overview of a new method addressed to study molecular solutes at the QM ab initio level, J. Mol. Struct. THEOCHEM. 464 (1999) 211–226. http/doi.org/10.1016/S0166-1280(98)00553-3.

[34] J. Tomasi, B. Mennucci, R. Cammi, Quantum mechanical continuum solvation models, Chem. Rev. 105 (2005) 2999–3094. http/doi.org/10.1021/cr9904009

[35] C. Eller, B.W. Smucker, R. Kirgan, D.M. Eichhorn, D.P. Rillema, 5,5'-Di-methyl-2,2'-bi-pyrazine, Acta Crystallogr. Sect. E. 60 (2004) o433--o434. http/doi.org/10.1107/S1600536804000881.

[36] H.-M. Wen, Y.-H. Wu, Y. Fan, L.-Y. Zhang, C.-N. Chen, Z.-N. Chen, Spectroscopic and Luminescence Studies on Square-Planar Platinum(II) Complexes with Anionic Tridentate 3-Bis(2-pyridylimino)isoindoline Derivatives, Inorg. Chem. 49 (2010) 2210–2221. http/doi.org/10.1021/ic902019s.

[37] L. Yi, L.-N. Zhu, B. Ding, P. Cheng, D.-Z. Liao, S.-P. Yan, Z.-H. Jiang, Six- and four-coordinated zinc(II) complexes exhibit strong blue fluorescent properties, Inorg. Chem. Commun. 6 (2003) 1209–1212. http/doi.org/10.1016/S1387-7003(03)00224-7.

[38] G.-G. Luo, D.-L. Wu, L. Liu, S.-H. Wu, D.-X. Li, Z.-J. Xiao, J.-C. Dai, A novel 1D T5(0)A(2) water tape incorporated in the channel of the first 3D silver-suberate framework, J. Mol. Struct. 1014 (2012) 92–96. http/doi.org/10.1016/J.MOLSTRUC.2012.02.003.

[39] R.-D. Schnebeck, E. Freisinger, F. Glahé, B. Lippert, Molecular Architecture Based

on Metal Triangles Derived from 2,2‘-Bipyrazine (Bpz) and EnMII (M = Pt, Pd), J. Am. Chem. Soc. 122 (2000) 1381–1390. http/doi.org/10.1021/ja9931325.

[40] E. Guney, V.T. Yilmaz, A. Sengul, O. Buyukgungor, Platinum(II) and palladium(II) saccharinato complexes with 2,2′:6′,2″-terpyridine: Synthesis, characterization, crystal structures, photoluminescence and thermal studies, Inorganica Chim. Acta. 363 (2010) 438–448. http/doi.org/10.1016/J.ICA.2009.11.018.

[41] V. Maheshwari, M. Carlone, F.R. Fronczek, L.G. Marzilli, Ligand and coordination-plane distortions in platinum(II) complexes of isomers of dimethyl-2,2'-bipyridine, Acta Crystallogr. Sect. B. 63 (2007) 603–611. http/doi.org/10.1107/S0108768107027024.

[42] T. Tian, I. Mutikainen, G.P. van Wezel, N. Aliaga-Alcalde, J. Reedijk, Chemical, structural and biological studies of cis-[Pt(3-Acpy)2Cl2], J. Inorg. Biochem. 103 (2009) 1221–1227. http/doi.org/10.1016/J.JINORGBIO.2009.06.009.

[43] R.D. Gillard, A. Sengül, A. Oldroyd, Dimorphism in a 2,2′,2″-terpyridyl compound, Transit. Met. Chem. 26 (2001) 339–344. http/doi.org/10.1023/A:1007120731989.

[44] A. Şengül, N. Karadayı, O. Büyükgüngör, *N* , *N* ′-Bis[1-(pyrazin-2-yl)ethylidene]hydrazine, Acta Crystallogr. Sect. C Cryst. Struct. Commun. 60 (2004) o507–o508. http/doi.org/10.1107/S010827010401220X.

[45] A. Şengül, Crystal Structure of Nitrato(2,2’,2’’-terpyridyl)platinum(II) Hydrogen Dinitrate, [Pt(terpy)ONO2][H(ONO2)2], Turkish J. Chem. 29 (2005) 571–578.

606 [46] C.S. Angle, A.G. DiPasquale, A.L. Rheingold, L.H. Doerrer, Red and yellow
607 solvates of chloro-(2,2':6',2''-terpyridine)platinum(II) chloride and Pt...Pt
608 interactions, Acta Crystallogr. Sect. C. 62 (2006) m340--m342.
609 http/doi.org/10.1107/S010827010601924X.

610 [47] R. Valiente, J.M. García-Lastra, P. García-Fernández, S. García-Revilla, O.S.
611 Wenger, Red-to-Yellow Pressure-Induced Phase Transition in Pt(bpy)Cl2:
612 Spectroscopic Study Supported by DFT Calculations, Eur. J. Inorg. Chem. 2007
613 (2007) 5735–5742. http/doi.org/10.1002/ejic.200700060.

614 [48] A. Sengül, Crystal and Molecular Structure of the Yellow Form of
615 Chloro(2,2' :6',2"-terpyridine)platinum (II)chloride dihydrate,
616 [Pt(terpy)Cl]Cl·2H2O, Turkish J. Chem. 28 (2004) 667–672.

617 [49] A. Şengül, W.-J. Wang, S.J. Coles, A novel dinuclear double-stranded helical
618 complexes of bis(terdentate) N4O2 donor ligand with silver(I) and zinc(II) d10
619 metal ions, Polyhedron. 28 (2009) 69–76.
620 http/doi.org/10.1016/J.POLY.2008.10.011.

621 [50] A. Sengul, O. Kurt, O. Buyukgungor, A 2D network silver coordination polymer
622 with the multimodal ligand 2-pyrazyl methyl ketazine, Struct. Chem. 22 (2011)
623 925–929. http/doi.org/10.1007/s11224-011-9778-z.